Molecular Mechanism of the *Thermus thermophilus* ADP-Ribose Pyrophosphatase from Mutational and Kinetic Studies†

Takushi Ooga,‡ Sachico Yoshiba,‡ Noriko Nakagawa,‡,§ Seiki Kuramitsu,‡,§ and Ryoji Masui*,‡,§

Department of Biology, Graduate School of Science, Osaka University, Toyonaka, Osaka 560-0043, Japan, and RIKEN Harima Institute/SPring-8, 1-1-1 Kouto, Mikazuki-cho, Sayo-gun, Hyogo 679-5148, Japan

Received January 13, 2005; Revised Manuscript Received April 30, 2005

ABSTRACT: ADP-ribose pyrophosphatase (ADPRase), a member of the nudix protein family, catalyzes the hydrolysis of ADP-ribose to AMP and ribose 5′-phosphate. We have determined the crystal structure of ADPRase from *Thermus thermophilus* HB8 (*Tt*ADPRase). We performed kinetic analysis of mutants of *Tt*ADPRase to elucidate the substrate recognition and the catalytic mechanism. Our results suggest that interactions responsible for the substrate recognition are located at the terminal moieties of the substrate. The adenine moiety is recognized by Ile-19 and the main chain carbonyl group of Glu-29 and/or Gly-104. The terminal ribose moiety is recognized by the sum of some weak interactions with multiple residues that are close in space. Glu-82 and Glu-86, conserved in the nudix motif, were previously shown to be essential for catalysis. Mutation of these residues shows that the dependence of k_{cat} on pH is almost the same as that of the wild-type enzyme. Results suggest that Glu-82 and Glu-86 are essential for catalysis but unlikely to act as a catalytic base. In the crystal structure, each acidic residue coordinates with a metal ion. Furthermore, a water molecule coordinates between these two metals. Our results suggest a two-metal ion mechanism for the catalysis of ADPRase in which a water molecule is activated to act as a nucleophile by the cations coordinated by Glu-82 and Glu-86. Arg-54, Glu-70, Arg-81, and Glu-85 are predicted to support this nucleophilic attack on the α-phosphate of the substrate. Interestingly, ADPRase displays differences in the substrate recognition and the catalytic mechanism from the models proposed for other nudix proteins. Our results highlight the diversity within the nudix protein family in terms of substrate recognition and catalysis.

Nudix pyrophosphatases are widely distributed in nature and have been identified from viruses to humans. These enzymes are characterized by the presence of a highly conserved sequence motif called the "nudix motif" [GX_5EX_7REUXEEXGU, where U is a bulky hydrophobic amino acid (I, L, or V)] (*1*). The nudix motif forms a loop−helix−loop structural motif that is involved in Mg^{2+} binding and catalysis (*2*−*4*). Enzymes in this protein family catalyze the hydrolysis of nucleoside diphosphate linked to another moiety X, in the presence of Mg^{2+} or any other divalent cation. It has been proposed that the cellular function of the nudix proteins is to remove damaged nucleotides or metabolic intermediates such as 8-oxo-dGTP (*5*), dinucleoside polyphosphates (*6*), or coenzymes (*7*, *8*).

ADP-ribose (ADPR)[1] is a substrate of the nudix proteins, and ADP-ribose pyrophosphatase (ADPRase) constitutes a major group of the nudix protein family. This enzyme catalyzes the hydrolysis of ADPR to AMP and ribose 5′-phosphate (R5P). ADPRase activity has been found in all three domains of life (*9*−*12*).

Recent studies have provided clues about the substrate recognition and the catalytic mechanism of ADPRase. The X-ray crystal structures of ADPRase from *Escherichia coli* (*Ec*ADPRase) (*4*), *Mycobacterium tuberculosis* (*Mt*ADPRase) (*13*), *Thermus thermophilus* HB8 (*Tt*ADPRase) (*14*), and *Homo sapiens* (NUDT9) (*15*) have been reported. On the basis of the Mg^{2+}−substrate ternary complex structure of *Ec*ADPRase, a catalytic model was proposed in which Glu-162, located outside the nudix motif, acts as a catalytic base (*16*). In a previous study, we determined the crystal structure of *Tt*ADPRase and analyzed the function of a Glu residue corresponding to Glu-162 in *Ec*ADPRase by site-directed mutagenesis. We found that the mutation at this site gave an active enzyme, suggesting that the catalytic residue is located elsewhere. On the basis of further structural and mutational analysis, we proposed a model in which the nudix motif and Glu-70 of *Tt*ADPRase are involved in catalysis (*14*).

In this study, we have prepared mutants of *Tt*ADPRase on the basis of its crystal structure and analyzed their activity. We have identified residues involved in substrate binding

† This work was supported in part by Grants-in-Aid for Scientific Research 13033025 (to S.K.) and 15570114 (to R.M.) from the Ministry of Education, Science, Sports and Culture of Japan.

* To whom correspondence should be addressed: Department of Biology, Graduate School of Science, Osaka University, Osaka, Japan. Telephone: +81-6-6850-5434. Fax: +81-6-6850-5442. E-mail: rmasui@bio.sci.osaka-u.ac.jp.

‡ Osaka University.

§ RIKEN Harima Institute/SPring-8.

[1] Abbreviations: ADPR, ADP-ribose; GDPR, GDP-ribose; CDPR, CDP-ribose; CIAP, calf intestine alkaline phosphatase; R5P, ribose 5′-phosphate; ADPRase, ADP-ribose pyrophosphatase; *Tt*ADPRase, *T. thermophilus* ADPRase; *Ec*ADPRase, *E. coli* ADPRase; *Mt*ADPRase, *M. tuberculosis* ADPRase; Ap_4Aase, diadenosine 5′,5‴-P^1,P^4-tetraphosphate; GDPMH, GDP-mannose mannosyl hydrolase; Ndx, nudix proteins from *T. thermophilus*; WT, wild-type.

10.1021/bi050078y CCC: $30.25
Published on Web 06/09/2005

and reveal a unique mode of substrate recognition displayed by the ADPRase group of enzymes. Furthermore, mutational and kinetic studies of residues conserved in the nudix motif have allowed us to propose a new catalytic model. This model differs from that proposed for other nudix proteins (*17*−*19*). Our paper demonstrates the diversity of molecular mechanisms exhibited by the nudix family of proteins.

EXPERIMENTAL PROCEDURES

Materials. ADPR and ADP-glucose (ADPG) were purchased from Sigma-Aldrich, and GDP-ribose (GDPR) and CDP-ribose (CDPR) were products of BIOLOG. Calf intestine alkaline phosphatase (CIAP) was purchased from TaKaRa. Primers used in the construction of mutants were synthesized by Greiner, PROLIGO, NIPPON EGT, BEX, and Invitrogen.

Overexpression and Purification. All mutations of *Tt*ADPRase were prepared by the method of Yoshiba for D126N (*14*) with some modification. KOD-plus-DNA polymerase (TOYOBO) was used for the PCRs. After the reaction, T4 DNA polymerase was added to complete the polymerase reaction. The pET-11a plasmid and the Rosetta-gami(DE3) strain (Novagen) were used for overexpression of *Tt*ADPRase and its mutants. The wild type (WT) and all mutant proteins were prepared by a previously described method (*20*) with some modifications. In this case, TOYOPEARL SuperQ-650 (Tosoh), TOYOPEARL Phenyl-650 (Tosoh), and Superdex 75 10/300 GL (Amersham Biosciences) columns were used for the chromatography after heat treatment.

Enzyme Assays. The assay used to assess the hydrolysis of the substrate was previously described (*14*, *21*). For measurement of ADPRase activity, the reaction mixture contained 50 mM Tris-HCl (pH 7.63), 100 mM KCl, 5 mM $MgCl_2$, 2 units/100 μL CIAP, 20−2000 nM enzyme, and 0−3 mM ADPR. For measurement of hydrolytic activity using NDP sugars, the reaction mixture contained 50 mM Tris-HCl (pH 7.63), 100 mM KCl, 20 mM $MgCl_2$, 5 units/100 μL CIAP, 50−100 nM enzyme, and 0−5 mM substrate. Reactions were performed at 25 °C for up to 10 h. The kinetic parameters were determined by fitting the data to the Michaelis−Menten equation using Igor Pro (WaveMetrics).

Dependence of k_{cat} on pH. The kinetic measurements of pK_a for WT and mutant enzymes were performed using MES-HCl buffer (pH 4.87, 5.43, 5.94, 6.49, and 6.98), Tris-HCl buffer (pH 7.03, 7.63, 8.19, 8.64, and 9.10), and glycine-NaOH buffer (pH 9.01, 9.56, 10.08, 10.38, and 10.72). The reaction mixture contained 50 mM buffer, 100 mM KCl, 20 mM $MgCl_2$, 5 units/100 μL CIAP, 10−10000 nM enzyme, and 0−10 mM ADPR. Reactions were performed at 25 °C for up to 20 h. Under these conditions, verification of the CIAP coupling assay was performed by HPLC analysis (data not shown).

The kinetic measurements of pK_a for the WT enzyme were performed in the presence of different divalent cations using MES-HCl buffer (pH 4.62, 5.27, 5.82, and 6.49) and Tris-HCl buffer (pH 6.90, 7.58, 8.10, 8.54, and 8.95). The reaction mixture (100 μL) contained 50 mM buffer, 100 mM KCl, 5 mM divalent cation ($MgCl_2$, $MnCl_2$, or $ZnCl_2$), 5−5000 nM enzyme, and 0−2 mM ADPR. Reactions were performed at 25 °C for up to 30 min. The reaction was stopped by adding an equal volume of 100 mM H_3PO_4. The protein was removed by ultrafiltration using a membrane filter (VIVASPIN VS0112 from VIVASCINCE). A 50 or 90 μL aliquot of the filtrate was applied to an anion exchange column (TSK-GEL DEAE-2SW, 4.6 mm × 75 mm, Tosoh) equilibrated with 50 mM sodium phosphate (pH 4.3) and 20% acetonitrile. Elution was performed on a linear gradient from 50 to 500 mM sodium phosphate. The substrate and one of the reaction products (AMP) were detected at 260 nm, and each concentration was calculated by integration of their respective peak area. The pK_a in the plot of k_{cat} against pH and $(k_{cat})^{max}$ were calculated as previously described (*22*).

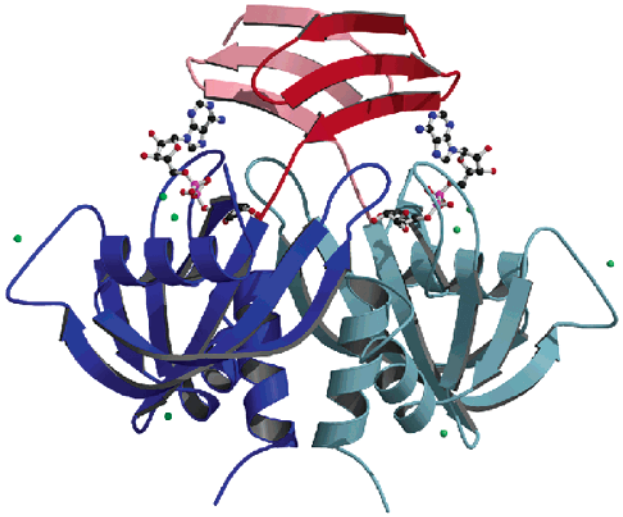

FIGURE 1: Overall structure of the *Tt*ADPRase−ADPR−Gd^{3+} ternary complex (PDB entry 1V8M) (*14*).

Fluoride Inhibition Measurement. The reaction mixture contained 50 mM Tris-HCl (pH 7.63), 100 mM KCl, 5 mM $MgCl_2$, 50 nM enzyme, 0−1 mM ADPR, and 0, 10, 50, or 100 μM NaF. Reactions were performed at 25 °C for up to 10 min. Quantification of reaction products was performed by a HPLC method as described above. From a Lineweaver−Burk plot for each inhibitor concentration, we assumed mixed inhibition (*23*) using eq 1.

$$v_0 = V_{max}[S]/[(1 + [I]/K_{i1})K_m + (1 + [I]/K_{i2})[S]] \quad (1)$$

K_{i1} and K_{i2} represent the inhibition constants for the free enzyme and for the Michaelis complex, respectively. The inhibition constants were obtained by fitting the initial rate of the product formation to eq 1.

RESULTS

Effect of Mutation on the Adenosine-Binding Site. Using the crystal structure of *Tt*ADPRase in complex with ADPR and Gd^{3+} as a guide, target residues were chosen for the site-directed mutagenesis to investigate the role of residues involved in substrate recognition and catalysis for *Tt*ADPRase. Purified WT and mutant enzymes were analyzed by steady-state kinetics, and the Michaelis−Menten parameters were determined.

ADPR is bound to the dimeric interface of *Tt*ADPRase (Figure 1). The adenine moiety of ADPR is located in the hydrophobic pocket composed of Arg-18, Ile-19, Arg-27*, and Tyr-28* (residue numbers of another subunit are indicated with asterisks in Figure 2A). Ile-19 and Tyr-28*

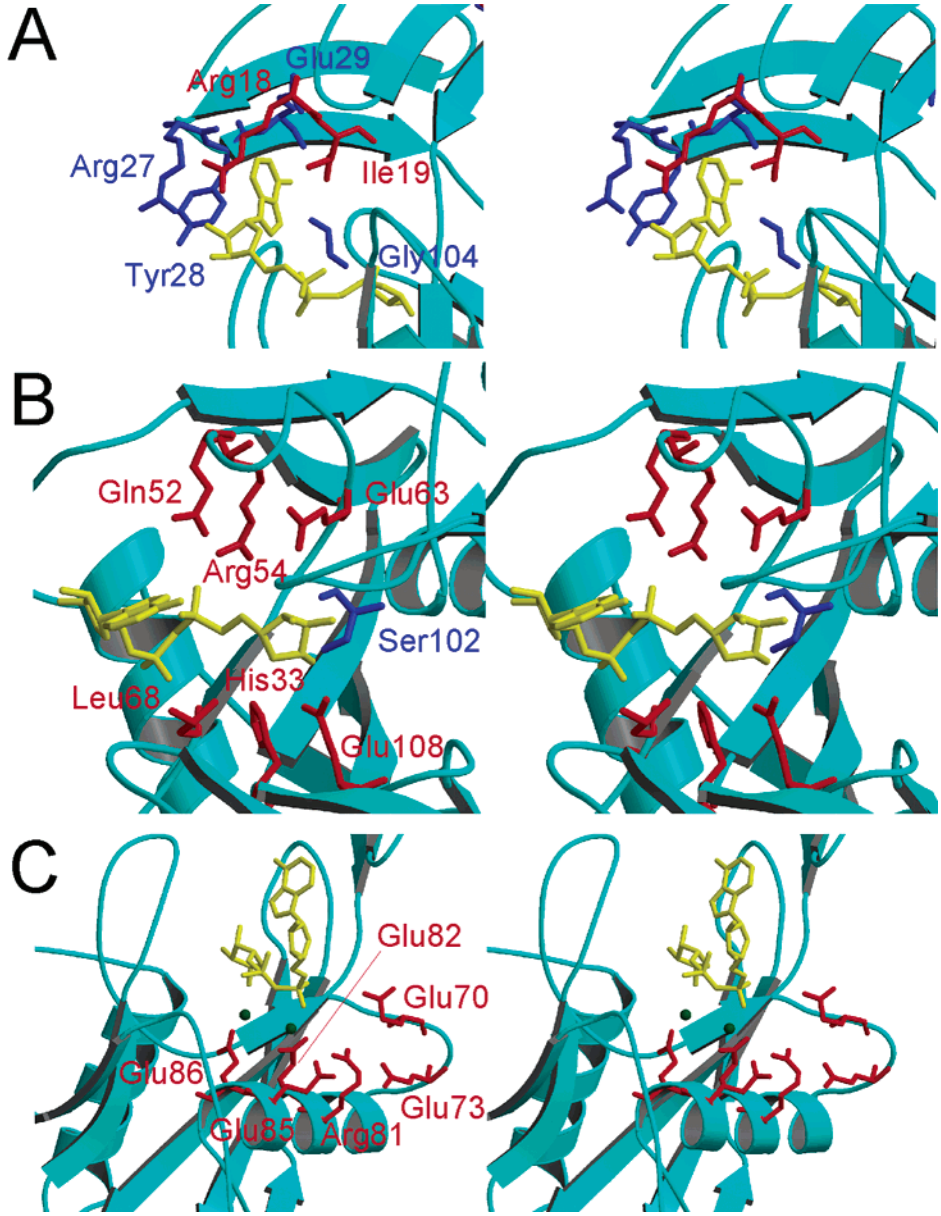

FIGURE 2: Structure of the *Tt*ADPRase−ADPR−Gd^{3+} ternary complex (PDB entry 1V8M). Putative substrate-interacting residues are shown in the stick model. Residues from each subunit are differently colored (red and blue). ADPR is colored yellow: (A) adenosine-binding site, (B) phosphate-binding site and terminal ribose-binding site, and (C) active site formed by residues in the nudix motif and Glu-70. Gd^{3+} ions are colored light green. These stereoviews are in the divergent-eye format.

are located on each side of the adenine ring. Arg-18 and Arg-27* seem to interact with the 2′-hydroxyl group (O2H) of the adenosyl ribose (3.5 and 2.5 Å, respectively). For the recognition of the adenine moiety, I19A exhibited an 11-fold increase in K_m in comparison with that of WT. This result indicates an important interaction between Ile-19 and the adenine moiety. In contrast, a small increase in K_m for Y28Q (3.6-fold) indicates no significant contribution of this residue in the recognition of the adenine moiety. The small changes in the k_{cat} values of these mutant enzymes (0.5- and 0.9-fold decrease for I19A and Y28Q, respectively) suggest that the hydrophobic interactions formed by these residues are involved only in substrate binding.

Furthermore, the crystal structure predicted another essential interaction that allows the enzyme to distinguish the adenine base from other bases. Specifically, this involves interactions between N6 of the adenine moiety and the main chain carbonyl group of Glu-29* or Gly-104* (2.8 or 2.8 Å, respectively) (Figure 2A). To verify this prediction, we assessed the activity of WT for the substrate analogues containing the guanine or the cytosine base (Table 2). A 10-fold increase in K_m for GDPR was observed, indicating the importance of the interactions between N6 of the adenine and the two carbonyl groups. Furthermore, the 12-fold increase in K_m for CDPR was almost the same as that for GDPR, suggesting that the structural difference between a purine and a pyrimidine is not essential for substrate recognition in *Tt*ADPRase.

The ribose moiety of the adenosine is almost outside the binding pocket (Figure 2A). Arg-18 and Arg-27* are likely to form interactions (3.5 and 2.5 Å, respectively) with its O2H. However, R18Q and R27Q* showed only a negligible increase (1.1- and 1.3-fold, respectively) in K_m (Table 1), suggesting that the adenosyl ribose moiety is not essential for substrate recognition. R18Q and R27Q exhibited an only slight increase in k_{cat} (1.1- and 1.3-fold increase, respectively),

Table 1: Kinetic Parameters of *Tt*ADPRase Mutants for ADPR

	K_m (mM)	k_{cat} (s^{-1})	k_{cat}/K_m (M^{-1} s^{-1})
WT	0.11 ± 0.02	10.65 ± 0.36	9.95×10^4
recognition of the adenosine moiety			
R18Q	0.12 ± 0.01	17.05 ± 0.22	1.48×10^5
I19A	1.24 ± 0.07	5.68 ± 0.23	4.58×10^3
R27Q	0.14 ± 0.04	12.90 ± 0.22	9.56×10^4
Y28Q	0.40 ± 0.03	10.04 ± 0.21	2.51×10^4
recognition of the phosphates and the terminal ribose moiety			
H33A	0.42 ± 0.06	4.16 ± 0.18	9.93×10^3
Q52A	0.24 ± 0.03	6.74 ± 0.24	2.86×10^4
R54Q	0.65 ± 0.06	$(4.11 \pm 0.10) \times 10^{-2}$	6.26×10
E63Q	0.40 ± 0.03	0.23 ± 0.01	5.75×10^2
L68A	0.31 ± 0.03	5.93 ± 0.13	1.89×10^4
S102A	0.69 ± 0.04	2.43 ± 0.05	3.51×10^3
E108Q	0.29 ± 0.02	2.97 ± 0.05	1.04×10^4
Y99F	0.09 ± 0.01	3.32 ± 0.04	3.77×10^4
T110A	0.06 ± 0.01	2.65 ± 0.04	4.30×10^4
S153A	0.10 ± 0.01	3.30 ± 0.06	3.44×10^4
T155A	0.05 ± 0.01	2.42 ± 0.03	5.25×10^4
catalysis			
E70Q	$(0.18 \pm 0.02) \times 10^{-1}$	0.41 ± 0.01	1.12×10^4
E73Q	$(0.36 \pm 0.07) \times 10^{-1}$	2.07 ± 0.08	5.64×10^4
R81Q	$(0.27 \pm 0.01) \times 10^{-1}$	$(3.50 \pm 0.28) \times 10^{-2}$	1.29×10^3
E82Q	0.11 ± 0.01	$(9.39 \pm 0.01) \times 10^{-4}$	8.42
E85Q	$(0.43 \pm 0.06) \times 10^{-1}$	1.12 ± 0.03	2.59×10^4
E86Q	0.10 ± 0.01	$(1.53 \pm 0.02) \times 10^{-3}$	1.48×10

Table 2: Kinetic Parameters of WT *Tt*ADPRase for NDP Sugars

	K_m (mM)	k_{cat} (s^{-1})	k_{cat}/K_m (M^{-1} s^{-1})
ADPR	0.11 ± 0.02	10.65 ± 0.36	9.95×10^4
GDPR	1.10 ± 0.13	3.57 ± 0.16	3.24×10^3
CDPR	1.36 ± 0.18	3.36 ± 0.14	2.48×10^3
ADPG	3.16 ± 0.63	9.10 ± 1.11	2.88×10^3

indicating no significant role for these residues in the catalytic mechanism.

Effect of the Mutation on the Phosphate-Binding Site and Terminal Ribose-Binding Site. The terminal ribose moiety of bound ADPR was the α-configuration and surrounded by several residues from both subunits (Figure 2B). In WT, replacement of the terminal ribose unit with glucose gave a 29-fold increase in K_m (Table 2). This result indicates significant interaction between the terminal ribose moiety and *Tt*ADPRase.

The structural data suggested that His-33, Glu-63, Ser-102*, and Glu-108 can directly interact with O1H, O2H, or O3H of the terminal ribose moiety (5.2, 5.9, 2.9, and 3.4 Å, respectively). Thus, the effect of mutation of these residues on the activity was assessed (Table 1). A 3.8-, 3.6-, 6.3-, and 2.6-fold increase in K_m was observed for H33A, E63Q, S102A, and E108Q, respectively. These results suggest that each interaction with the terminal ribose moiety is relatively weak. In addition, we assessed the effect of the mutation of Tyr-99, Thr-110, Ser-153, and Thr-155, which can interact with O1H or O2H of the terminal ribose moiety via only a water molecule. The distances are as follows: 5.3 Å between Tyr-99 and O1H, 4.5 Å between Thr-110 and O1H, 5.8 Å between Ser-153 and O2H, and 5.6 Å between Thr-155 and O2H. A small change in the K_m of each mutant enzyme (0.8-, 0.6-, 0.9-, and 0.5-fold decrease for Y99F, T110A, S153A, and T155A, respectively) suggests that these residues are not significantly involved in binding to the terminal ribose moiety.

A slight decrease in k_{cat} was observed when mutations were introduced at almost all residues located near the terminal ribose moiety. These results indicate that some interactions in the terminal ribose binding pocket contribute to catalysis. The only exception is seen in E63Q, which exhibited a 46.4-fold decrease in k_{cat}. Analysis by circular dichroism (200−250 nm) of all the mutants showed that only E63Q exhibited a spectrum distinct from that of WT. Therefore, the large decrease in k_{cat} for E63Q is probably due to the partial destruction of its secondary or tertiary structure.

The side chain of Gln-52 and Arg-54 can interact with the α- and β-phosphates of the substrate, respectively. Leu-68 is located close to these two phosphates (Figure 2B). Q52A, R54Q, and L68A exhibited 2.2-, 5.9-, and 2.8-fold increases in K_m, respectively. These results suggest that the interaction between Arg-54 and the β-phosphate is important for substrate recognition. Furthermore, R54Q exhibited a 260-fold decrease in k_{cat}, suggesting that Arg-54 is directly involved in the catalysis.

Effect of Mutation on Residues in the Active Site. In *Tt*ADPRase, the nudix motif (residues 67−89) forms a loop−helix structure. The highly conserved residues in the nudix motif and Glu-70 form the active site (Figure 2C). In our previous study, the mutation of Glu-82 and Glu-86, which coordinate two metal ions in the active site, showed a severe decrease in k_{cat} (5.2×10^4- and 3.8×10^4-fold decrease for E82Q and E86Q, respectively), indicating the important role of these residues in catalysis (*14*). To further elucidate the contribution of the residues in the active site to substrate recognition and catalysis, we mutated the highly conserved residues in the nudix motif and Glu-70 and assessed the effect on the activity (Table 1). E82Q and E86Q exhibited 1.1×10^4- and 7.0×10^3-fold decreases in k_{cat}, respectively. The slight discrepancy in the value between the previous and current studies is probably due to changes in the purification procedure.

R81Q showed a drastic decrease in k_{cat} (304-fold), indicating the important role of Arg-81 during catalysis. In the crystal structure, Arg-81 can interact with Glu-85 and Glu-82, and the latter (Glu-82) coordinates a metal ion in the active site (Figure 2C). Therefore, Arg-81 is predicted to make important contributions to catalysis via Glu-82.

Although Glu-70 is not a conserved residue in the nudix motif, it is highly conserved among ADPRase enzymes as either Glu or Asp. In the *Tt*ADPRase−ADPR−Zn^{2+} ternary complex structure, Glu-70 accepts a hydrogen bond from a water molecule, which could be a candidate for a nucleophile. We previously proposed a reaction mechanism in which Glu-70 acts as a catalytic base by activating the nucleophilic water molecule (*14*). To verify this hypothesis, we prepared E70Q and found an only 26-fold decrease in k_{cat}. This decrease seems to be too small to account for the contribution of Glu-70 as a general base in catalysis. Although we still consider this residue to be important in catalysis, our previous model for the catalytic mechanism needs to be modified.

Glu-73 is one of the highly conserved residues in the nudix motif. Nevertheless, E73Q showed an only slight change in k_{cat} (5.1-fold decrease). In the crystal structure, Glu-73 is far from the active site but close to the helix containing the nudix motif residues. These observations suggest that Glu-73 plays a role in stabilizing the structure of the active site.

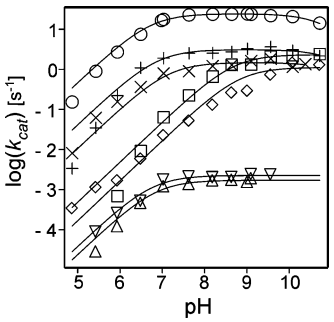

FIGURE 3: pH dependence of k_{cat}: WT (○), R54Q (□), E70Q (×), R81Q (◇), E82Q (△), E85Q (+), and E86Q (▽). The theoretical curves were calculated with Igor Pro using the parameters given in Table 3.

Table 3: Parameters Calculated from the pH Dependence of k_{cat}

	pK_{H2ES}	pK_{HES}	$(k_{cat})^{max}$ (s^{-1})
WT	6.71 ± 0.04	10.84 ± 0.06	24.37 ± 0.40
R54Q	8.68 ± 0.10		2.32 ± 0.11
E70Q	7.19 ± 0.21	(>11.00)[a]	1.48 ± 0.12
R81Q	8.92 ± 0.01		1.12 ± 0.11
E82Q	6.86 ± 0.10		(1.71 ± 0.06) × 10^{-3}
E85Q	6.89 ± 0.13	(>11.00)[a]	3.12 ± 0.15
E86Q	6.78 ± 0.12		(2.26 ± 0.10) × 10^{-3}

[a] The values could not be determined precisely because the data were not obtained above pH 11.

Glu-85 is another highly conserved residue, although some nudix proteins have different residues at this position [e.g., GDP-mannnose mannosyl hydrolase (GDPMH) from *E. coli*]. In *Tt*ADPRase, Glu-85 can interact with Arg-81 or a water molecule, and the latter can also interact with Glu-70, Glu-82, or a metal ion. The 9.5-fold decrease in k_{cat} for E85Q indicates that Glu-85 makes some contribution to catalysis, but it is not a catalytic base itself.

Mutation of residues in the nudix motif and Glu-70 resulted in no significant change in K_m (0.02-, 0.3-, 0.2-, 1.0-, 0.4-, and 0.9-fold decreases for E70Q, E73Q, R81Q, E82Q, E85Q, and E86Q, respectively). In the crystal structure, these residues have no direct interaction with the substrate. Therefore, the small decreases in K_m for E70Q, E73Q, R81Q, and E85Q are probably due to destabilization of the transition state in comparison with the substrate-binding state.

pH Dependence of k_{cat}. To further investigate the roles of residues in the active site, we assessed the pH dependence of k_{cat} for WT and several mutants (R54Q, E70Q, R81Q, E82Q, E85Q, and E86Q) (Figure 3 and Table 3). These mutations involved residues that were predicted to play a role in catalysis.

For WT *Tt*ADPRase, two pK_a values were obtained as seen in other nudix proteins (*17*, *22*). The value of pK_{H2ES} (6.7) indicates the existence of a group with a pK_a at neutral pH. His is a possible candidate, but *Tt*ADPRase has no His residue in the active site. Another candidate for this group is a Glu in the active site or a water molecule coordinated by metal ions. The other value of pK_{HES} (10.8) is close to the pK_a value of Lys or Arg. There are two Arg residues (Arg-54 and Arg-81) in the active site.

Calculated values of pK_{H2ES} and pK_{HES} for mutants are shown in Table 3. We were unable to perform measurements in the high-pH range for mutants E82Q and E86Q because of the high rate of spontaneous substrate degradation. Similarly for mutants R54Q and R81Q, we could not determine the pK_{HES} values and the corresponding descending limbs. For this reason, the pK_{H2ES} values of these four mutants were calculated by fitting the data to a single dissociation equation. For E70Q and E85Q, both descending limbs were identified. However, the pK_{HES} value could not be determined due to the high rate of spontaneous degradation of the substrate above pH 11.

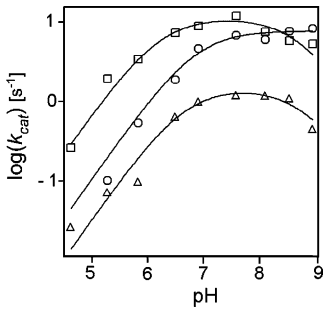

FIGURE 4: pH dependence of k_{cat} in the presence of Mg^{2+}, Mn^{2+}, or Zn^{2+}: Mg^{2+} (○), Mn^{2+} (△), and Zn^{2+} (□). The values of pK_{H2ES} and pK_{HES} were calculated by fitting the data to a single (Mg^{2+}) and double (Mn^{2+} and Zn^{2+}) dissociation equation. The values of pK_{H2ES} were 6.86 ± 0.12 (Mg^{2+}), 6.67 ± 0.14 (Mn^{2+}), and 6.24 ± 0.20 (Zn^{2+}). The values of pK_{HES} were 8.79 ± 0.15 (Mn^{2+}), 8.71 ± 0.19 (Zn^{2+}). The values of $(k_{cat})^{max}$ were 7.34 ± 0.38 (Mg^{2+}), 1.42 ± 0.14 (Mn^{2+}), and 10.97 ± 1.22 (Zn^{2+}). The theoretical curves were calculated with Igor Pro using the above parameters.

Although both E82Q and E86Q exhibited a drastic decrease in $(k_{cat})^{max}$ (1.4×10^4- and 1.1×10^3-fold, respectively) their pK_{H2ES} values (6.9 and 6.8, respectively) were almost the same as that of WT (6.7). These results suggest that although Glu-82 and Glu-86 are essential for catalysis, they do not play a role as a general base. However, the pK_{H2ES} values of R54Q and R81Q shifted significantly to a higher pH (8.7 and 8.9, respectively), with a large decrease in $(k_{cat})^{max}$ (10.5- and 21.8-fold, respectively). The pK_{H2ES} values of E70Q and E85Q (7.2 and 6.9, respectively) were close to that of WT. Their pK_{HES} values were not determined precisely.

pH Dependence of k_{cat} for Different Cations. To demonstrate the importance of divalent cations in catalysis, we assessed the pH dependence of k_{cat} for WT in the presence of Mg^{2+}, Mn^{2+}, or Zn^{2+} (Figure 4). In the presence of Mg^{2+}, we could not determine the pK_{HES} value and the corresponding descending limb. Therefore, the pK_{H2ES} value was calculated by fitting the data to a single dissociation equation (6.86 ± 0.12). In the presence of Mn^{2+} and Zn^{2+}, both values of pK_{H2ES} and pK_{HES} were determined. The pK_{H2ES} values for Mn^{2+} and Zn^{2+} were 6.67 ± 0.14 and 6.24 ± 0.20, respectively (i.e., significantly lower than that for Mg^{2+}). The pK_{HES} values for Mn^{2+} and Zn^{2+} could be calculated to be 8.79 ± 0.15 and 8.71 ± 0.19, respectively. The values of $(k_{cat})^{max}$ were 7.34 ± 0.38 (Mg^{2+}), 1.42 ± 0.14 (Mn^{2+}), and 10.97 ± 1.22 (Zn^{2+}).

Inhibition by Fluoride Ions. WT *Tt*ADPRase was extremely sensitive to the inhibition by F^- via a mixed inhibition mechanism. Inhibition constants (K_{i1} and K_{i2}) from eq 1 (see Experimental Procedures) were determined to be 150 and 15 μM, respectively.

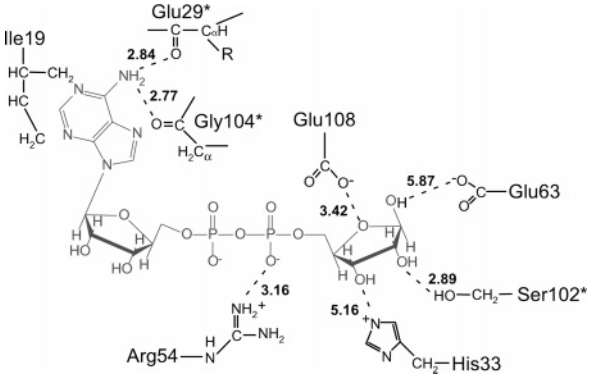

FIGURE 5: Model of primary interactions involved in the substrate recognition of *Tt*ADPR. Numbers represent distances between the respective atoms (angstroms) in PDB entry 1V8M. Residue numbers of another subunit are indicated by the asterisks.

DISCUSSION

Currently, the crystal structures of four ADPRases have been determined (*4*, *13*−*15*). On the basis of these structural data, models for substrate recognition and the catalytic mechanism have been proposed (*14*, *16*). However, there are insufficient kinetic and mutational studies of these enzymes to verify these hypotheses. Elucidation of the molecular mechanism of ADPRase will also be valuable for the analysis of other nudix proteins. The data presented here reveal the detailed role of several residues involved in substrate recognition and catalysis.

An overview of the substrate recognition mechanism of *Tt*ADPRase is presented in Figure 5. In the crystal structure, the conformation of the bound ADPR resembles a horseshoe. Almost all putative interactions between the enzyme and ADPR are localized around the adenine and terminal ribose moieties of the substrate (*4*, *14*). Two primary interactions for the recognition of the adenine moiety were revealed in this study. We found that Ile-19 plays a major role in recognizing the base, presumably through a hydrophobic interaction. Another primary interaction is the hydrogen bond between N6 of the adenine and the main chain carbonyl group of Glu-29* and/or Gly-104*. Although these interactions made by the carbonyl groups of the main chain could not be confirmed experimentally, there are no other likely candidates (Figure 2A and Table 2).

Mutational analysis suggests that there are no critical interactions for the recognition of the terminal ribose moiety. Although His-33, Glu-63, Ser-102*, and Glu-108 form hydrogen bonds with the terminal ribose, these interactions were shown to be weak. Nevertheless, *Tt*ADPRase displayed strict specificity for the terminal ribose moiety (Table 2). Therefore, this strong specificity should be ascribed to the sum of these weak interactions. Mutation of residues around the terminal ribose-binding site always resulted in a slight decrease in k_{cat} (Table 1). Furthermore, two residues, His-33 and Glu-63, are distant from the substrate in the crystal structure (5.2 and 5.9 Å, respectively). These residues may contribute to the catalysis by relocating the terminal ribose moiety in the transition state.

In addition to the two terminal moieties, only the β-phosphate is likely to be recognized by Arg-54. This interaction may also play an important role in the catalysis. The α-phosphate group and ribose moiety of the adenosine moiety are less important in substrate recognition.

Recently, the crystal structures of ADPRase from *E. coli* (*4*) and *M. tuberculosis* (*13*) were determined in ternary complexes with the substrate and metal ions. Here again, the terminal moieties of the substrate are thought to be important in substrate recognition. Slight, but nevertheless important, differences were observed. For example, the corresponding residue of Ile-19 in *Tt*ADPRase is Phe (-28) in *Ec*ADPRase. However, the recognition mechanism is thought to be common among these ADPRases. The crystal structure of NUDT9 from *H. sapiens* was also determined (*15*). Although the substrate recognition mechanism for this monomeric ADPRase is interesting, the structure with the substrate has not yet been obtained. This makes it difficult to compare the substrate recognition mechanism of NUDT9 with that of *Tt*ADPRase.

Crystal or solution structures have been determined for several other groups of nudix proteins with strict substrate specificity. For some of them, the substrate recognition mechanisms have been studied by kinetic, mutational, and NMR analyses. The MutT pyrophosphohydrolase from *E. coli* is the most studied enzyme among the nudix proteins. MutT has an especially high specificity for its substrate, 8-oxo-dGTP, compared with that of the substrate analogue dGTP (*5*). The NMR study revealed that two hydrogen bonds between the purine ring of the substrate and two residues, Asn-119 and Arg-78, contribute to this specificity (*24*). In the case of the diadenosine tetraphosphate pyrophosphohydrolase (Ap_4Aase) from *Caenorhabditis elegans*, structural (*25*) and mutational studies (*26*) revealed that P^1-phosphate of the substrate interacts with some residues, and this interaction is essential for substrate recognition. One adenine moiety of the substrate is stacked between the side chains of two Tyr residues, but this stacking interaction is not as important for substrate recognition. GDPMH is an unusual member of the nudix protein family, which hydrolyzes GDP-mannose to GDP and mannose. From the crystal structure with its product GDP (*27*), the substrate recognition mechanism of GDPMH seems to resemble that of ADPRase. For example, the guanine moiety is surrounded by a hydrophobic pocket, which is formed from several N-terminal residues, and the main chain carbonyl and amino groups of Leu-4 interact with N2 and O6 of the guanine base, respectively. However, GDPMH has an additional mechanism for substrate recognition. For example, the guanine base is stacked between two Tyr residues, and the α-phosphate interacts with Arg-65 (corresponding to Arg-81 of *Tt*ADPRase) via a water molecule. Thus, each nudix protein group appears to have a different substrate recognition mechanism. Importantly, however, the residues constituting the nudix motif make no contribution to substrate recognition (Table 1).

The crystal structure of *Ec*ADPRase with a nonhydrolyzable substrate suggested that Glu-162, located in the L9 loop, may act as a catalytic base to activate a water molecule (*16*). In the case of *Mt*ADPRase, mutation of Glu-142, corresponding to Glu-162 in *Ec*ADPRase, resulted in a 3.2-fold increase in K_m and a 300-fold decrease in k_{cat} (*19*). However, our previous mutational study was inconsistent with this hypothesis, and instead proposed a catalytic role for Glu-70 (*14*). Both residues are situated outside the nudix motif. However, in this study, the E70Q mutant exhibited an only 5-fold decrease in k_{cat}, suggesting that Glu-70 cannot act as the catalytic base. The most effective change in k_{cat} was

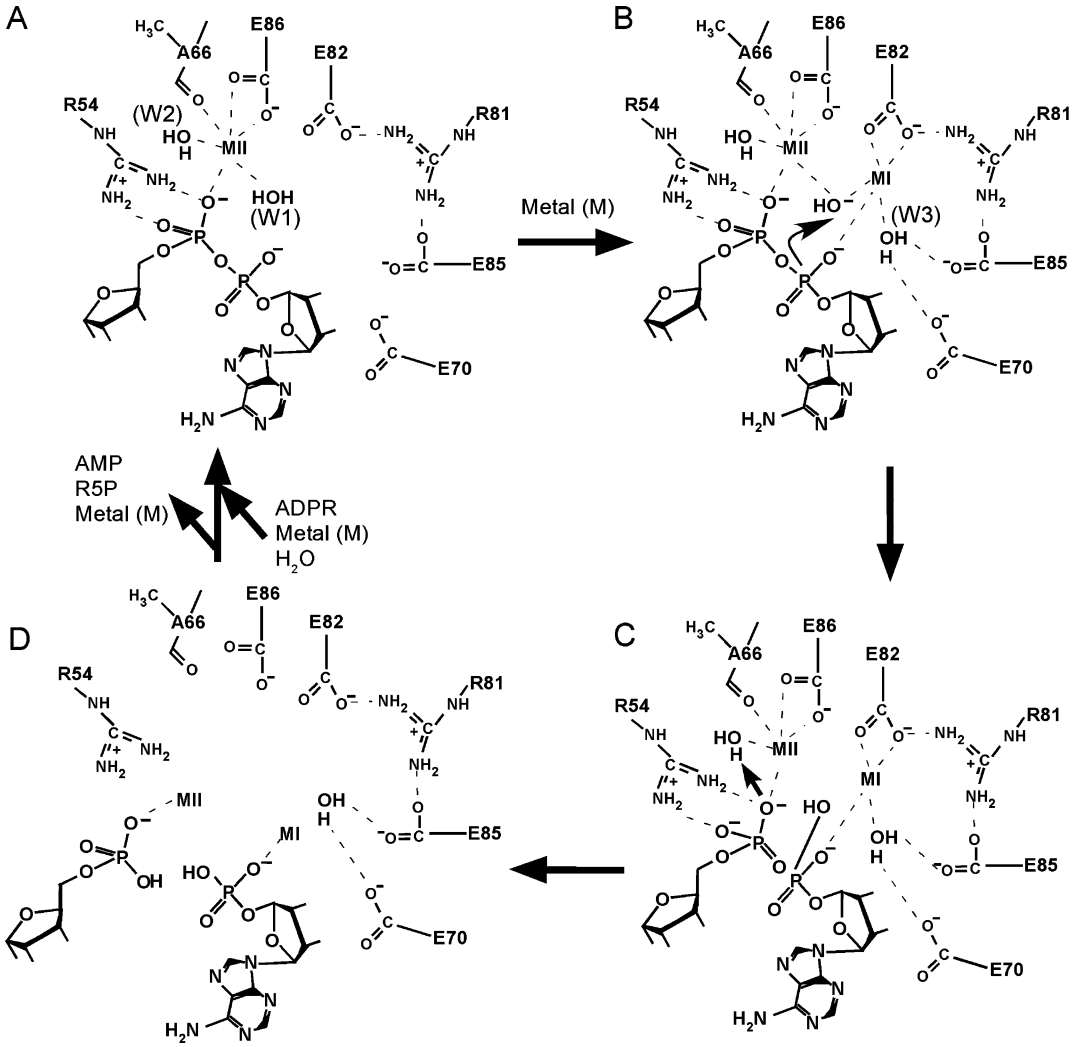

FIGURE 6: Proposed model of the catalytic mechanism of *Tt*ADPRase. (A) Single cation-binding state. (B) Ternary complex with ADPR and two cations. In this state, cations activate a water molecule (WI). (C) Transition state. (D) Product-release state. The nucleophilic attack and proton abstraction events are shown with arrows.

observed for mutants of Glu-82 and Glu-86, which are conserved in the nudix motif. These results suggest that Glu-82 and Glu-86 play an essential role in the catalytic mechanism. The importance of these two conserved residues has also been suggested in other nudix proteins (*17*, *22*, *25*). In particular, Glu-53 of *E. coli* MutT, corresponding to Glu-82 of *Tt*ADPRase, was demonstrated to act as a catalytic base to activate the nucleophilic water molecule.

To verify the role of Glu-82, Glu-86, and other residues located in the active site, we examined the pH dependence of k_{cat} for each mutant. In the ADPRase reaction, it was demonstrated that a solvent water molecule is activated to attack the α-phosphate group (*14*, *16*). Therefore, replacement of the catalytic residue was predicted to generate a mutant showing significant changes in pK_{HES} or pK_{H2ES}. E82Q and E86Q mutants showed a drastic decrease in $(k_{cat})^{max}$, but surprisingly, their pK_{H2ES} values were almost the same as that of WT (Table 3). This result suggests that although Glu-82 and Glu-86 are essential for catalysis, they do not act as a catalytic base.

In *Tt*ADPRase, two metal ions are coordinated between the substrate and the residues in the active site of the enzyme−ADPR−Gd^{3+} ternary complex (*14*). One metal (MI) is coordinated by Glu-82, and the other (MII) is coordinated to Glu-86 and the main chain carbonyl group of Ala-66 (Figure 6). In contrast, the crystal structure of the ternary complex of ADPRase from *E. coli* and *M. tuberculosis* shows three divalent cations are coordinated in the active site (*13*, *16*). Two of these cations are located at positions similar to the positions of the two metal ions in *Tt*ADPRase. Therefore, coordination of two divalent cations in the active site appears to be a common feature among ADPRases. This coordination resembles that of the two-metal ion mechanism found in DNA polymerases (*28*) and inorganic pyrophosphatases (*29*). In this mechanism, a water molecule coordinated by two cations has an extremely low pK_a (*30*) and can act as a nucleophile. On the basis of the similarity in cation coordination, ADPRase is also thought to use a two-metal ion mechanism, which involves a cluster composed of a water molecule (W1) and two divalent cations (MI and MII). If this is the case, the pK_{H2ES} value of WT (6.7) could be interpreted as the abnormally lowered pK_a of the coordinated water molecule.

In this model, we demonstrate the almost identical pK_{H2ES} values for WT, E82Q, and E86Q. From the crystal structure, E86Q has only one divalent cation (Zn^{2+}) (MI) coordinated by Glu-82 (*14*). A drastic decrease in $(k_{cat})^{max}$ for E86Q is likely to be the result of a collapse of the catalytic cluster.

FIGURE 7: Sequence alignment of the nudix motifs in three representative nudix proteins. The nudix motif sequences of ADPRase (*Tt*ADPRase), MutT (*E. coli* 8-oxo-dGTPase), and GDPMH (*E. coli* GDP-mannose mannosyl hydrolase) were aligned using ClustalW. The numbers correspond to the residues in each enzyme.

Surprisingly, E86Q has almost the same pK_{H2ES} (6.8) as WT (6.7) (Table 3). This observation may be rationalized as follows. MI and W1 are still coordinated in E86Q by the interaction with Glu-82. When MII is located at an appropriate position in the active site, even without interaction with any residues, W1 is coordinated by MI and MII and is sufficiently activated to attack the α-phosphate of the substrate. This situation is also applicable to E82Q, which showed a drastically lowered $(k_{cat})^{max}$ but the same value of pK_{H2ES} (6.9) as WT. In this case, MI is substituted with MII, which is coordinated to Glu-86.

Arg-81 of *Tt*ADPRase corresponds to Arg-52 of MutT. For MutT, Arg-52 is thought to interact with catalytic base Glu-53 (*19*), although the distance between them is more than 10 Å. In this study, the marked decrease in $(k_{cat})^{max}$ for R81Q suggests an essential role for Arg-81 during catalysis. In addition, R81Q exhibited a drastic shift of pK_{H2ES} to a higher value (8.9) compared to that of WT. We initially predicted that Arg-81 acts as a proton donor because Arg is generally protonated at neutral pH. However, considering the pK_{H2ES} shift to a higher value in R81Q, this seems unlikely. Because Arg-81 can interact directly with Glu-82 and Glu-85 (2.94 and 2.86 Å, respectively), it is possible that the catalytic role of Arg-81 is mediated by these residues. However, neither E82Q nor E85Q showed a pK_{H2ES} shift equivalent to that of R81Q, and this scenario is also unlikely. Our results suggest that Arg-81 may act as a positive charge donor. The active site of *Tt*ADPRase is composed of many negative charges (i.e., the phosphate groups and several Glu residues). Arg-81, together with the divalent cations, may provide a positive charge to lower the pK_a of the nucleophilic water. Loss of the positive charge in R81Q may cause a decrease in $(k_{cat})^{max}$ and a shift in the pK_{H2ES} through disruption of the charge balance.

R54Q also exhibited a considerable pK_{H2ES} shift to a higher value in comparison to that of WT. Therefore, Arg-54 appears to act in the same way as Arg-81 in functioning as a positive charge donor. In addition, Arg-54 seems to stabilize negative charges of the β-phosphate during substrate binding and formation of the transition state (Figure 6). Lys-39 of MutT is structurally equivalent to Arg54 of *Tt*ADPRase. This residue is proposed to act as a Lewis acid to promote the departure of the leaving group. Therefore, Arg-54 may have the same function as Lys-39 of MutT. Although, in this case, there would be some change in the value of pK_{HES} for R54Q compared with that of WT, we could not determine the value of pK_{HES} for R54Q.

Glu-70 and Glu-85 are also located in the active site, but the mutation of these residues resulted in an only slight decrease in $(k_{cat})^{max}$ and almost the same pK_{H2ES} value as that of WT. These results suggest that Glu-70 and Glu-85 contribute indirectly to catalysis. As Glu-70 cannot interact with the nucleophilic water or the divalent cations directly, it is probable that Glu-70 is involved in the coordination of one divalent cation (MI) via an intervening water molecule (W3) (Figure 6). A similar situation seems to exist for Glu-85, although this residue is positioned more closely to the active site than Glu-70. Mutation of residues located near the cations also leads to an upshift in pK_a for inorganic pyrophosphatase from *E. coli*, which is thought to possess a two-metal ion mechanism (*30*).

The difference in $(k_{cat})^{max}$ for various divalent cations suggests that the activity of *Tt*ADPRase is significantly influenced by the species of divalent cation. Furthermore, the values of pK_{H2ES} for WT were significantly different: 6.9 for Mg^{2+}, 6.7 for Mn^{2+}, and 6.2 for Zn^{2+}. It is noteworthy that the order of these values ($Mg^{2+} > Mn^{2+} > Zn^{2+}$) is consistent with that of acid ionization (hydrolysis) constants for these cations: 11.4 for Mg^{2+}, 10.5 for Mn^{2+}, and 9.7 for Zn^{2+} (*31*, *32*). This result indicates that the catalytic property depends on the character of the divalent cations coordinating in the active site, and also strongly supports our hypothesis that *Tt*ADPRase uses a two-metal ion mechanism for catalysis.

The inhibition effect of F^- on ADPRase activity means that F^- inhibits both substrate binding and catalysis. Inhibition of substrate binding ($K_{i1} = 150$ μM) is thought to result from competition between ADPR and F^- in binding Mg^{2+}. The significant inhibition of catalysis ($K_{i2} = 15$ μM) is presumably caused by F^- occupying the nucleophile site between the two divalent cations in the active site. Fluoride ion inhibition was also observed for inorganic pyrophosphatase (*33*), implying an essential role for the Mg^{2+}-bound hydroxide ion in the catalysis of a two-metal ion mechanism. For other nucleotide hydrolases, fluoride ion inhibition is known to be caused by the formation of the transition-state analogue $X-Mg^{2+}-(F^-)_3-O-NDP$ complex (*34*). The same mechanism of inhibition is proposed for nudix hydrolases (*19*). At present, there is no direct experimental evidence to support either hypothesis for fluoride inhibition of nudix proteins.

On the basis of these results, we propose a new model for the catalytic mechanism of *Tt*ADPRase (Figure 6). In this model, the nucleophile is the cluster of a water molecule (W1) and two divalent cations (MI and MII) that are coordinated by Glu-82 and Glu-86 (and Ala-66). Figure 6A represents the substrate-binding state with one divalent cation (in Figure 6, MII is coordinated mainly by Glu-86). In this state, nucleophilic attack does not occur because the activation of W1 is insufficient. However, once another divalent cation (in Figure 6, MI which is coordinated mainly by Glu-82) is appropriately positioned (Figure 6B), W1 is rendered sufficiently nucleophilic by two divalent cations and the loss of one proton and attacks the α-phosphate (*14*). The

β-phosphate is temporarily stabilized by Arg-54, and accepts a proton from a water molecule (W2) (Figure 6C). Figure 6D shows the release of the products, AMP and R5P.

In addition to ADPRase, a detailed reaction mechanism has been proposed for MutT and GDPMH (*17*, *18*). Mutation of Glu-53 in *E. coli* MutT, corresponding to Glu-82 of *Tt*ADPRase (Figure 7), resulted in a loss in pK_{H2ES} (*17*). NMR studies of MutT showed that two divalent cations are essential for its activity (*35*). However, only one of them is coordinated to the acidic residues of the enzyme. In the proposed model, Glu-53, corresponding to Glu-82 of *Tt*ADPRase, activates a water molecule coordinating to a divalent cation. pK_{H2ES} (7.7) represents the deprotonation of Glu-53. GDPMH, which catalyzes an unusual reaction as a nudix protein (*36*), lacks a Glu corresponding to Glu-82 of *Tt*ADPRase (Figure 7) (*36*). Surprisingly, the catalytic base of GDPMH is His-124, located outside the nudix motif (*18*, *27*). GDPMH requires only one divalent cation for its activity, which is coordinated to Glu-70 corresponding to Glu-86 of *Tt*ADPRase (*37*). In contrast, it has been shown that Ap_4Aase requires three divalent cations for its activity, and two of them are located between the substrate and the enzyme (*38*). The catalytic model of Ap_4Aase resembles that for *Tt*ADPRase proposed in this study but not that of MutT (*19*). Therefore, a difference in the coordination of the divalent cations at the active site appears to give rise to a divergent catalytic mechanism in the nudix protein family, despite the existence of a common catalytic motif (*19*).

Further experiments are required to verify the proposed mechanism described in this paper. Nevertheless, this study confirms that groups of nudix proteins show diversity not only in terms of substrate recognition but also in the detailed mechanism of catalysis. Nudix proteins appear to be unique in possessing a common catalytic motif but a different mechanism of action. Structural and functional studies of other Ndx proteins from *T. thermophilus* HB8 are in progress to investigate their molecular mechanism.

ACKNOWLEDGMENT

We thank Hirofumi Omori for technical assistance in DNA sequencing for the mutant enzymes in this study.

REFERENCES

1. Bessman, M. J., Frick, D. N., and O'Handley, S. F. (1996) The MutT proteins or "Nudix" hydrolases, a family of versatile, widely distributed, "housecleaning" enzymes, *J. Biol. Chem. 271*, 25059−25062.
2. Abeygunawardana, C., Weber, D. J., Gittis, A. G., Frick, D. N., Lin, J., Miller, A. F., Bessman, M. J., and Mildvan, A. S. (1995) Solution structure of the MutT enzyme, a nucleoside triphosphate pyrophosphohydrolase, *Biochemistry 34*, 14997−15005.
3. Lin, J., Abeygunawardana, C., Frick, D. N., Bessman, M. J., and Mildvan, A. S. (1997) Solution structure of the quaternary MutT-M^{2+}-AMPCPP-M^{2+} complex and mechanism of its pyrophosphohydrolase action, *Biochemistry 36*, 1199−1211.
4. Gabelli, S. B., Bianchet, M. A., Bessman, M. J., and Amzel, L. M. (2001) The structure of ADP-ribose pyrophosphatase reveals the structural basis for the versatility of the Nudix family, *Nat. Struct. Biol. 8*, 467−472.
5. Maki, H., and Sekiguchi, M. (1992) MutT protein specifically hydrolyses a potent mutagenic substrate for DNA synthesis, *Nature 355*, 273−275.
6. McLennan, A. G. (1999) The MutT motif family of nucleotide phosphohydrolases in man and human pathogens, *Int. J. Mol. Med. 4*, 79−89.
7. Xu, W., Dunn, C. A., and Bessman, M. J. (2000) Cloning and characterization of the NADH pyrophosphatases from *Caenorhabditis elegans* and *Saccharomyces cerevisiae*, members of a Nudix hydrolase subfamily, *Biochem. Biophys. Res. Commun. 273*, 753−758.
8. Cartwright, J. L., Gasmi, L., Spiller, D. G., and McLennan, A. G. (2000) The *Saccharomyces cerevisiae PCD1* gene encodes a peroxisomal nudix hydrolase active toward coenzyme A and its derivatives, *J. Biol. Chem. 275*, 32925−32930.
9. Sheikh, S., O'Handley, S. F., Dunn, C. A., and Bessman, M. J. (1998) Identification and characterization of the Nudix hydrolase from the Archaeon, *Methanococcus jannaschii*, as a highly specific ADP-ribose pyrophosphatase, *J. Biol. Chem. 273*, 20924−20928.
10. Ingram, S. W., Stratemann, S. A., and Barnes, L. D. (1999) *Schizosaccharomyces pombe* Aps1, a diadenosine 5′,5″-P1, P6-hexaphosphate hydrolase that is a member of the nudix (MutT) family of hydrolases: Cloning of the gene and characterization of the purified enzyme, *Biochemistry 38*, 3649−3655.
11. O'Handley, S. F., Frick, D. N., Dunn, C. A., and Bessman, M. J. (1998) Orf186 represents a new member of the Nudix hydrolases, active on adenosine(5′)triphospho(5′)adenosine, ADP-ribose, and NADH, *J. Biol. Chem. 273*, 3192−3197.
12. Yang, H., Slupska, M. M., Wei, Y. F., Tai, J. H., Luther, W. M., Xia, Y. R., Shih, D. M., Chiang, J. H., Baikalov, C., Fitz-Gibbon, S., Phan, I. T., Conrad, A., and Miller, J. H. (2000) Cloning and characterization of a new member of the Nudix hydrolases from human and mouse, *J. Biol. Chem. 275*, 8844−8853.
13. Kang, L. W., Gabelli, S. B., Cunningham, J. E., O'Handley, S. F., and Amzel, L. M. (2003) Structure and mechanism of MT-ADPRase, a nudix hydrolase from *Mycobacterium tuberculosis*, *Structure 11*, 1015−1023.
14. Yoshiba, S., Ooga, T., Nakagawa, N., Shibata, T., Inoue, Y., Yokoyama, S., Kuramitsu, S., and Masui, R. (2004) Structural insights into the *Thermus thermophilus* ADP-ribose pyrophosphatase mechanism via crystal structures with the bound substrate and metal, *J. Biol. Chem. 279*, 37163−37174.
15. Shen, B. W., Perraud, A. L., Scharenberg, A., and Stoddard, B. L. (2003) The crystal structure and mutational analysis of human NUDT9, *J. Mol. Biol. 332*, 385−398.
16. Gabelli, S. B., Bianchet, M. A., Ohnishi, Y., Ichikawa, Y., Bessman, M. J., and Amzel, L. M. (2002) Mechanism of the *Escherichia coli* ADP-ribose pyrophosphatase, a Nudix hydrolase, *Biochemistry 41*, 9279−9285.
17. Harris, T. K., Wu, G., Massiah, M. A., and Mildvan, A. S. (2000) Mutational, kinetic, and NMR studies of the roles of conserved glutamate residues and of lysine-39 in the mechanism of the MutT pyrophosphohydrolase, *Biochemistry 39*, 1655−1674.
18. Legler, P. M., Massiah, M. A., and Mildvan, A. S. (2002) Mutational, kinetic, and NMR studies of the mechanism of *E. coli* GDP-mannose mannosyl hydrolase, an unusual Nudix enzyme, *Biochemistry 41*, 10834−10848.
19. Mildvan, A. S., Xia, Z., Azurmendi, H. F., Saraswat, V., Legler, P. M., Massiah, M. A., Gabelli, S. B., Bianchet, M. A., Kang, L.-W., and Amzel, L. M., (2005) Structures and mechanisms of Nudix hydrolases, *Arch. Biochem. Biophys. 433*, 129−143.
20. Yoshiba, S., Nakagawa, N., Masui, R., Shibata, T., Inoue, Y., Yokoyama, S., and Kuramitsu, S. (2003) Overproduction, crystallization and preliminary diffraction data of ADP-ribose pyrophosphatase from *Thermus* thermophilus HB8, *Acta Crystallogr. D59*, 1840−1842.
21. Ames, B. N., and Dubin, D. T. (1960) The role of polyamines in the neutralization of bacteriophage deoxyribonucleic acid, *J. Biol. Chem. 235*, 769−775.
22. Iwai, T., Kuramitsu, S., and Masui, R. (2004) The Nudix hydrolase Ndx1 from *Thermus thermophilus* HB8 is a diadenosine hexaphosphate hydrolase with a novel activity, *J. Biol. Chem. 279*, 21732−21739.
23. Fersht, A. R. (1999) *Structure and Mechanism in Protein Science*, W. H. Freeman and Co., New York.
24. Massiah, M. A., Saraswat, V., Azurmendi, H. F., and Mildvan, A. S. (2003) Solution structure and NH exchange studies of the MutT pyrophosphohydrolase complexed with Mg^{2+} and 8-oxo-dGMP, a tightly bound product, *Biochemistry 42*, 10140−10154.
25. Bailey, S., Sedelnikova, S. E., Blackburn, G. M., Abdelghany, H. M., Baker, P. J., McLennan, A. G., and Rafferty, J. B. (2002) The crystal structure of diadenosine tetraphosphate hydrolase from *Caenorhabditis elegans* in free and binary complex forms, *Structure 10*, 589−600.

26. Abdelghany, H. M., Bailey, S., Blackburn, G. M., Rafferty, J. B., and McLennan, A. G. (2003) Analysis of the catalytic and binding residues of the diadenosine tetraphosphate pyrophosphohydrolase from *Caenorhabditis elegans* by site-directed mutagenesis, *J. Biol. Chem. 278*, 4435−4439.
27. Gabelli, S. B., Bianchet, M. A., Azurmendi, H. F., Xia, Z., Sarawat, V., Mildvan, A. S., and Amzel, L. M. (2004) Structure and mechanism of GDP-mannose glycosyl hydrolase, a Nudix enzyme that cleaves at carbon instead of phosphorus, *Structure 12*, 927−935.
28. Beese, L. S., and Steitz, T. A. (1991) Structural basis for the 3′−5′ exonuclease activity of *Escherichia coli* DNA polymerase I: A two metal ion mechanism, *EMBO J. 10*, 25−33.
29. Heikinheimo, P., Lehtonen, J., Baykov, A., Lahti, R., Cooperman, B. S., and Goldman, A. (1996) The structural basis for pyrophosphatase catalysis, *Structure 4*, 1491−1508.
30. Salminen, T., Kapyla, J., Heikinheimo, P., Kankare, J., Goldman, A., Heinonen, J., Baykov, A. A., Cooperman, B. S., and Lahti, R. (1995) Structure and function analysis of *Escherichia coli* inorganic pyrophosphatase: Is a hydroxide ion the key to catalysis? *Biochemistry 34*, 782−791.
31. Basolo, F., and Pearson, R. G. (1958) *Mechanisms of inorganic reactions: A study of metal complexes in solution*, Chapman & Hall, London.
32. Dean, J. A. (1985) *Lange's Handbook of Chemistry*, McGraw-Hill, New York.
33. Smirnova, I. N., and Baikov, A. A. (1983) Two-stage mechanism of the fluoride inhibition of inorganic pyrophosphatase using the fluoride ion, *Biokhimiia 48*, 1643−1653.
34. Graham, D. L., Lowe, P. N., Grime, G. W., Marsh, M., Rittinger, K., Smerdon, S. J., Gamblin, S. J., and Eccleston, J. F. (2002) MgF_3^- as a transition state analogue of phospholyl transfer, *Chem. Biol. 9*, 375−381.
35. Frick, D. N., Weber, D. J., Gillespie, J. R., Bessman, M. J., and Mildvan, A. S. (1994) Dual divalent cation requirement of the MutT dGTPase. Kinetic and magnetic resonance studies of the metal and substrate complexes, *J. Biol. Chem. 269*, 1794−1803.
36. Legler, P. M., Massiah, M. A., Bessman, M. J., and Mildvan, A. S. (2000) GDP-mannose mannosyl hydrolase catalyzes nucleophilic substitution at carbon, unlike all other Nudix hydrolases, *Biochemistry 39*, 8603−8608.
37. Legler, P. M., Lee, H. C., Peisach, J., and Mildvan, A. S. (2002) Kinetic and magnetic resonance studies of the role of metal ions in the mechanism of *Escherichia coli* GDP-mannose mannosyl hydrolase, an unusual nudix enzyme, *Biochemistry 41*, 4655−4668.
38. Conyers, G. B., Wu, G., Bessman, M. J., and Mildvan, A. S. (2000) Metal requirements of a diadenosine pyrophosphatase from *Bartonella bacilliformis*: Magnetic resonance and kinetic studies of the role of Mn^{2+}, *Biochemistry 39*, 2347−2354.

BI050078Y